Cavities in Proteins: Structure of a Metmyoglobin–Xenon Complex Solved to 1.9 Å†

Robert F. Tilton, Jr., Irwin D. Kuntz, Jr.,* and Gregory A. Petsko*

ABSTRACT: X-ray crystallographic data to 1.9-Å resolution were collected on sperm whale metmyoglobin equilibrated with 7 atm of xenon gas. The results indicate four xenon sites of occupancy from 0.45 to 1.0. These sites are located in interior spaces or packing defects of the myoglobin molecule. The effects of the bound xenon on the protein structure are minor, and we observe a small overall reduction in refined isotropic atomic protein temperature factors. We interpret the results as a confirmation that, on a time-averaged basis, cavities exist within the myoglobin molecule and suggest that the binding of small ligands in these cavities affects the internal motions and conformational substates of the protein.

The atomic positions revealed by X-ray diffraction of sperm whale myoglobin crystals define not only the static structure of the myoglobin molecule but also a characteristic arrangement of interior space (Richards, 1977; Connolly, 1981). Computational methods suggest that this space consists of a number of localized interior cavities with radii greater than 1.2 Å, which are connected to the protein surface and to other internal cavities by a larger number of small channels of radii less than 0.8 Å. These cavities are generally bounded by hydrophobic residues, range in size from 30 to 100 Å^3 and are located primarily in regions where helices pack against other helices or where helices pack against the prosthetic heme group. The term "packing defect" has been used to describe these internal cavities; however, it is still unclear whether they are solely structural anomalies or are important in the dynamics and function of the myoglobin molecule. While the distal cavity provides the necessary environment for reversible O_2 binding and has been studied in some detail, the other cavities are poorly understood. One method of investigating these cavities is to study the binding of specific probes. One such probe is xenon.

Xenon, a relatively large and hydrophobic atom, is known to bind to myoglobin. Early X-ray crystallographic reports indicated a xenon site in the proximal cavity opposite the heme group from the O_2 binding site. This site was found to be almost fully occupied in metmyoglobin (Schoenborn et al., 1965), deoxymyoglobin (Schoenborn & Nobbs, 1966), and alkaline myoglobin (Schoenborn, 1969). A second lower occupancy xenon site was also observed in alkaline myoglobin in the A–B, G–H corner region, a site which was similar to that observed in the hemoglobin α and β chains (Schoenborn, 1965). However, solution binding studies (Ewing & Maestas, 1970) suggest and ^{129}Xe NMR studies (Tilton & Kuntz, 1982) confirm the existence of at least two classes of xenon binding sites in both metmyoglobin and deoxymyoglobin. The NMR evidence indicates that one class of sites is near the iron and can be displaced with HgI_3^- while the second group of sites is distant from the iron with an NMR signal similar to that of Xe bound to hemoglobin. To determine the xenon sites and occupancies more precisely and to study the effects of bound xenon on the protein structure, we have collected X-ray crystallographic data to 1.9 Å and refined a model of metmyoglobin equilibrated with 7 atm of xenon gas.

Experimental Procedures

Crystal Preparation. Lyophilized sperm whale metmyoglobin was purchased from Sigma, and ultrapure ammonium sulfate was purchased from Bethesda Research Laboratories. Sperm whale metmyoglobin crystals were grown from 75% saturated ammonium sulfate, pH 6.9 at 18 °C (Kendrew & Parrish, 1956). The crystals were rectangular in shape, measuring 0.6 × 0.4 × 0.3 mm. Standard 0.7-mm quartz capillaries (Charles Supper Co.) were used to mount the crystal between two layers of cotton fibers wetted with a small amount of mother liquor. The capillary was then attached to a syringe containing Xe gas (AIRCO, 99.999% purity) and flushed with 4–5 volumes of gas before the narrow end was sealed with a microflame torch. The sealed end of the capillary was then immersed in liquid nitrogen, and approximately 7 volumes of xenon gas was allowed to distill in. Flame sealing near the top of the capillary and removal from the nitrogen bath caused pressurization to 7 atm within seconds. The total time for this procedure was approximately 2–3 min. A failure rate of 70% was attributed mainly to exploding capillaries caused by overpressurization and crystal damage due to freezing and heating. After successful pressurization, the flame-sealed ends were coated with "5-min" epoxy for added mechanical stability and allowed to equilibrate for 12 h at room temperature and an additional 12 h at 0 °C on the diffractometer. A schematic of the pressurizing apparatus is shown in Figure 1.

Data Collection. Data collection was performed on a Nicolet P3 diffractometer device using Ni-filtered Cu Kα radiation of wavelength 1.54 Å. A modified LT-1 temperature device maintained the temperature to ±1 °C with a cold N_2 stream at 0 °C during equilibration and data collection. A complete set of unique reflections to 1.9-Å resolution was collected by use of the fully integrating background–peak–background ω-step scan procedure. The total scan time per reflection was 20 s with an additional 8 s spent on background. A set of five standard reflections, evenly distributed through reciprocal space, was collected every 300 reflections as a monitor of crystal stability and radiation damage. Subsequently, for comparison with the metmyoglobin–Xe complex a complete set of native metmyoglobin data was measured at 270 K to 1.9-Å resolution on a different crystal.

Data Reduction. The measured intensities were corrected for background, absorption, and radiation damage (North et

† From the Department of Pharmaceutical Chemistry, University of California, San Francisco, San Francisco, California 94143 (R.F.T. and I.D.K.), and the Chemistry Department, Massachusetts Institute of Technology, Cambridge, Massachusetts 02139 (G.A.P.). *Received September 15, 1983; revised manuscript received December 15, 1983.* This work was supported by NIH Grants GM-19267 and GM-31497 (I.D.K.) and GM-26788 (G.A.P.). R.F.T. was an NIH trainee (GM-07175-06). Computer graphics pictures were made in the Computer Graphics Laboratory at UCSF (NIH RR-1081).

0006-2960/84/0423-2849$01.50/0

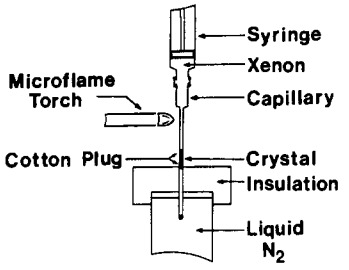

FIGURE 1: Schematic of the apparatus used to prepare metmyoglobin crystals pressurized to 7 atm with xenon gas.

al., 1968). Lorentz and polarization corrections were applied and a unique set of structure amplitudes was generated. These were scaled to previously measured structure amplitudes of a metmyoglobin crystal at 250 K. This data set was chosen as the "native" data set for the initial difference Fourier calculations because it was closest in temperature to the metmyoglobin–Xe measurements and had already been completely refined with 2-Å data to an R fractor of 0.19 (R. F. Tilton, I. D. Kuntz, G. A. Petsko, D. Ringe, and D. Rose, unpublished results). A difference electron density map was computed by using difference amplitudes of the form $F_{Mb+Xe(270)} - F_{Mb(250)}$ and phase angles from this refined 250 K metmyoglobin structure.

Refinement. The starting model for the metmyoglobin–Xe complex consists of the four xenon coordinates, as determined from the difference maps, appended to the refined 250 K metmyoglobin structure. Solvent and sulfate ions were explicitly omitted. These coordinates were further refined against the metmyoglobin–Xe structure factor amplitudes by a restrained least-squares procedure (Konnert & Hendrickson, 1980). To determine the occupancies and B factors for the four xenon atoms more precisely, a least-squares refinement using only the heavy xenon atoms was performed. Protein phase angles and F_{calcd} from the last cycle of refinement omitting the xenon atoms were used. Positions, occupancies, and B factors for the xenon atoms only were refined by adding the calculated xenon contribution vectorially to these calculated F's and minimizing the sum of the squares of the differences between these summed F_{calcd}'s and the measured F_{obsd}. Next, with these physicially sensible occupancies, refinement of xenon occupancies alone using fixed temperature factors was performed in each of eight resolution shells from 4.5 to 1.9 Å. Plots of ln (refined occupancy) vs. $\sin^2(\theta/\lambda^2)$ were used to adjust individual xenon B's. The occupancies were refined again with these adjusted B's and finally all xenon parameters were allowed to vary. These B's and occupancies for the xenon atoms were then held nearly constant (applied shift 0.01) in a final restrained refinement of the entire metmyoglobin–Xe structure.

Surface Calculations. Interior surfaces were calculated by the Connolly algorithm using probe sizes of 1.0, 1.1, 1.2, 1.3, and 1.4 Å. Essentially this algorithm produces the molecular surface that is accessible to the probe sphere (Connolly, 1983). Three coordinate sets were used: metmyoglobin (270 K) (Mb), metmyoglobin–Xe (270 K) with xenons present (Mb + Xe), and metmyoglobin–Xe (270 K) with xenons absent (Mb – Xe). Interior cavities were separated from the exterior surface by a clustering routine, and volumes were calculated by integration over the solid angle (Connolly, 1981; M. L. Connolly and N. Max, unpublished experiments). United atom approximations using implicit hydrogens were used for the aliphatic and aromatic carbon atoms while explicit hydrogens were used for the H-bonding oxygens and nitrogens. The water coordinated to the Fe in the distal cavity was removed for visualization of this site. A total of 1528 atoms were used in these calculations. The van der Waals radii for the individual atom types are as follows: carbonyl carbon, aromatic carbon, and methine carbon, 1.95 Å; methylene carbon, 2.00 Å; methyl carbon, 2.10 Å; hydrogen, 1.10 Å; nitrogens, 1.85 Å; oxygen, 1.70 Å; iron and xenon, 2.00 Å.

Results

Data Collection and Reduction. The metmyoglobin–Xe crystal has the symmetry of space group $P2_1$ with unit cell dimensions a = 64.23 (03) Å, b = 30.81 (01) Å, and c = 34.68 (02) Å and β = 105.77 (04)°. These dimensions are similar to those reported in the literature for metmyoglobin (Takano, 1977) and vary at most by 0.05 Å in cell dimension and 0.03° in β from the reference metmyoglobin crystal without Xe at 270 K. Before data collection the effect of the pressurization procedure on the integrity of the crystal was checked by examining reflection shape. Reflections were observed to be symmetrical with a half-width of 0.3° on ω scans. This value is typical of myoglobin crystals and indicates that no additional crystal disorder was caused by our pressurization procedure. A total of 10 105 unique reflections were collected to 1.9-Å resolution. Of these, 7165 had intensities greater than twice their standard deviation and were used in subsequent refinement steps. Decay of the measured intensities of the standard reflections was linear with time, independent of resolution, and indicated a radiation damage rate in intensity of 0.39%/h over a total of 80 h. After corrections and scaling, the mean fractional isomorphous difference between metmyoglobin–Xe (270 K) and metmyoglobin (250 K) was 0.17.

Difference Synthesis and Data Refinement. The Mb–Xe (270 K) – Mb (250 K) difference maps are relatively clean and clearly demonstrate four positive electron density features corresponding to four different xenon sites (Figure 2). The fractional coordinates of the highest density site correspond to the xenon position observed in earlier metmyoglobin–Xe crystallographic studies (Schoenborn et al., 1965). With inclusion of these four xenon sites in the coordinate list, the initial R factor was 36.4% with 400 out of 3511 bond distances more than two standard deviations from ideality (σ for bond lengths is set to 0.03 Å and σ for distances corresponding to bond angles is 0.04 Å). After 16 cycles of coordinate refinement only, the R factor decreased to 26.3% with 218 nonideal distances. Refinement with individual B factors for an additional 10 cycles and with individual B factors and variable Xe occupancies for three cycles dropped the R further to 20.9% with 156 nonideal bond distances, but left us with highly correlated and possibly inaccurate occupancies and B factors for the xenon sites. Refining the xenon sites separately as described gave similar results for B factors and occupancies as the general refinement. (These results were checked by substituting false xenon sites that refined to zero occupancy within two cycles.) The corrected occupancies when fixed in the protein refinement decreased the R to 19.2% with 121 nonideal bond distances using data from 4.1 to 1.9 Å and to 20.9% with 124 nonideal bond distances using data from 7.0 to 1.9 Å. The only B factor that varied significantly during the final four cycles of general refinement was the B factor for xenon 2, and even this was within twice its standard deviation. A final difference map, $F_{Mb+Xe,obsd} - F_{Mb+Xe,calcd}$, indicated no electron density at the four xenon positions but did reveal positive electron density at two known sulfate ion sites and a number of bound exterior waters, which had not been included in the refinement. The "native" metmyoglobin (270 K) data set was refined by the same method to an R factor of 19.1% with 120 deviant bond distances. All further

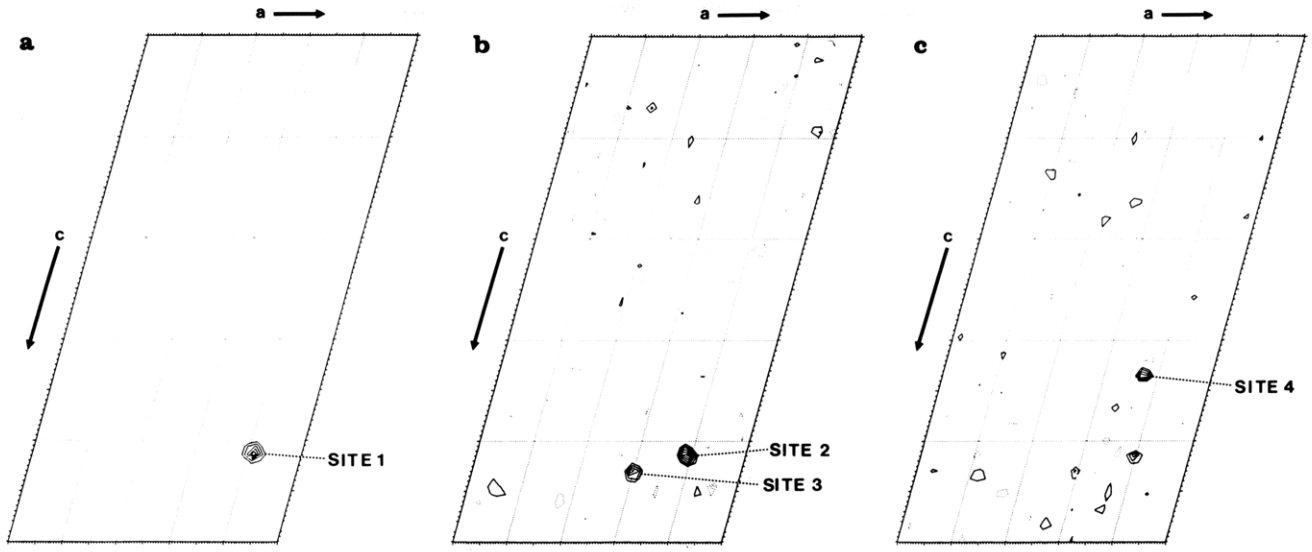

FIGURE 2: Difference electron density maps of metmyoglobin–xenon (270 K) and metmyoglobin (250 K). Xenon 1 is shown in (a). Contours are drawn at intervals of ±0.4 e Å^3 or 6σ. Xenon 2, xenon 3, and xenon 4 are indicated in (b) and (c). Contours are drawn at intervals of ±0.1 e Å^3 with negative contours shown with dashes. Note the extension of xenon site 2 and 3 in (c). The crystallographic axes *a* and *c* are indicated while the planes are perpendicular to the *b* axis. In (a), $b = 0.366$, (b), $b = 0.167$, and (c), $b = 0.200$. The refined coordinates are given in Table I.

Table I: Refined Fractional Coordinates, Occupancies, and *B* Factors for the Four Xenon Atoms

	fractional coordinates			occupancy	*B* factor (Å^2)
	a	*b*	*c*		
xenon 1	0.174	0.865	0.179	0.94	18.9
xenon 2	0.168	0.661	0.211	0.57	49.6
xenon 3	0.138	0.667	0.404	0.48	28.9
xenon 4	0.333	0.710	0.257	0.46	30.7

Table II: Calculated Volume for Internal Cavities[a]

radius (Å) probe size	volume (Å^3) Mb (270)[b]	Mb + Xe (270)[c]	Mb − Xe (270)[d]
1.0	489.3	282.7	482.9
1.1	369.5	200.9	401.9
1.2	240.7	104.4	289.1
1.3	196.6	42.1	226.1
1.4	141.2	23.8	145.5

[a] The Connolly algorithm was used to generate the surfaces and calculate internal cavity volumes (Connolly, 1981; M. L. Connolly and N. Max, unpublished experiments). [b] Metmyoglobin (270 K). [c] Metmyoglobin–Xe (270 K) with the xenons present during the surface calculation. [d] Metmyoglobin–Xe (270 K) with the xenons absent during the surface calculation.

comparisons use this as the reference structure.

Refined Structure. The refined coordinates, occupancies, and temperature factors for the xenon atoms are given in Table I. Xenon 1 is bound in the proximal pocket and is essentially fully occupied. The other three sites of lower occupancy, not observed in earlier crystallographic reports, also fill interior cavities. Xenon 2 has nearly the same *x* and *z* coordinates as xenon 1 and binds directly below the proximal cavity in a relatively small cavity near the bottom of the heme group. Xenon 3 resides in a cavity formed by the E–F helix corner and the H helix near the surface of the protein, while xenon 4 binds on the distal side of the molecule directly below the O_2 binding site. A model showing these four xenon sites is given in Figure 3, and a comparison of the interior cavity surfaces for Mb (270 K), Mb + Xe (270 K), and Mb − Xe (270 K) is shown in Figure 4. The cavity volumes are tabulated in Table II. Note that the xenon atoms occupy a large percentage of the calculated free interior space. To illustrate the individual binding sites, van der Waals surfaces (Bash et al., 1983) for the xenon atom and surrounding side chains are shown in Figure 5. Only xenon 2 is observed to have excessively close protein contacts. To quantify these nearest-neighbor contacts, atomic distances between the xenon atom and protein atoms, which are less then 5 Å, are given as supplementary material (see paragraph at end of paper regarding supplementary material). The only two close contacts are between xenon 2 and the ring atoms CE1 (2.78 Å) and CD1 (2.47 Å) of phenylalanine-138 (H14).

The overall effect of the bound xenons on the myoglobin structure is small, as reflected by a root mean square (rms) deviation between metmyoglobin–Xe (270 K) and metmyoglobin (270 K) of 0.28 Å for all atoms and only 0.14 Å for backbone atoms (C_α, C, N). The largest average side-chain deviations generally occur for the charged residues on the exterior surface of the protein although two interior side chains also exhibit large positional changes (Figure 6). These residues are leucine-89 (F4) and isoleucine-142 (H18), and both are found to have close contacts with xenon 1. An examination of the deviations for individual protein atoms near a xenon atom reveals that the largest deviations are neighbors or nearest neighbors of a xenon atom and that the protein has generally moved so as to allow for a larger Xe binding cavity (Table III).

The effect of the bound xenons on the individual atomic temperature factors of the myoglobin molecule can be investigated by comparing the average *B* factor for side-chain and backbone atoms of each residue for both metmyoglobin–Xe (270 K) and metmyoglobin (270 K) structures (Figure 7). While we observe a small average decrease (13%) for both the backbone and side-chain atom temperature factors, there are structural regions and individual residues that are affected to a much larger degree. In particular, the temperature factors associated with the B, the G, and the latter half of the A and H helices as well as the CD, EF, and FG corners are more affected while the E, the F, and first half of the H helix are nearly unaffected by xenon binding. A notable exception in the F helix is histidine-93 (F8), which shows a large decrease in temperature factor and neighbors xenon 1. The average *B* factor for the side chains parallels that for the backbone

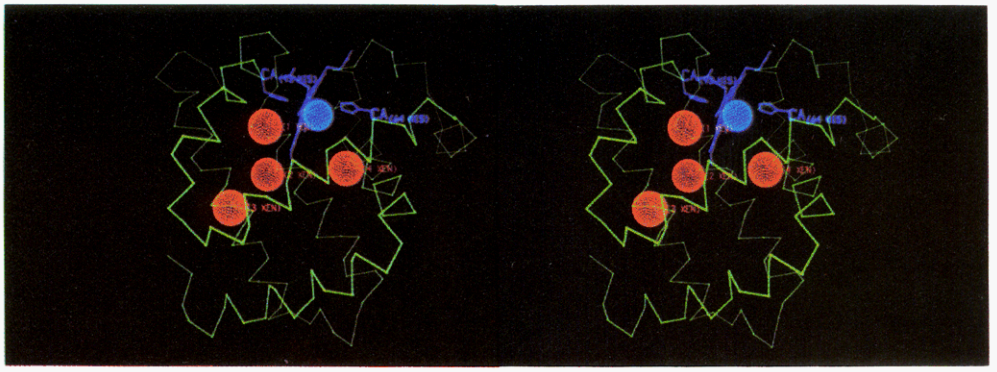

FIGURE 3: Refined metmyoglobin–xenon structure with the four xenon locations shown as red spheres. The C_α backbone is shown in green. The heme group, proximal histidine (93), and distal histidine (64) are shown in purple. The water molecule in the distal pocket is shown in blue. The proximal cavity is occupied by xenon 1.

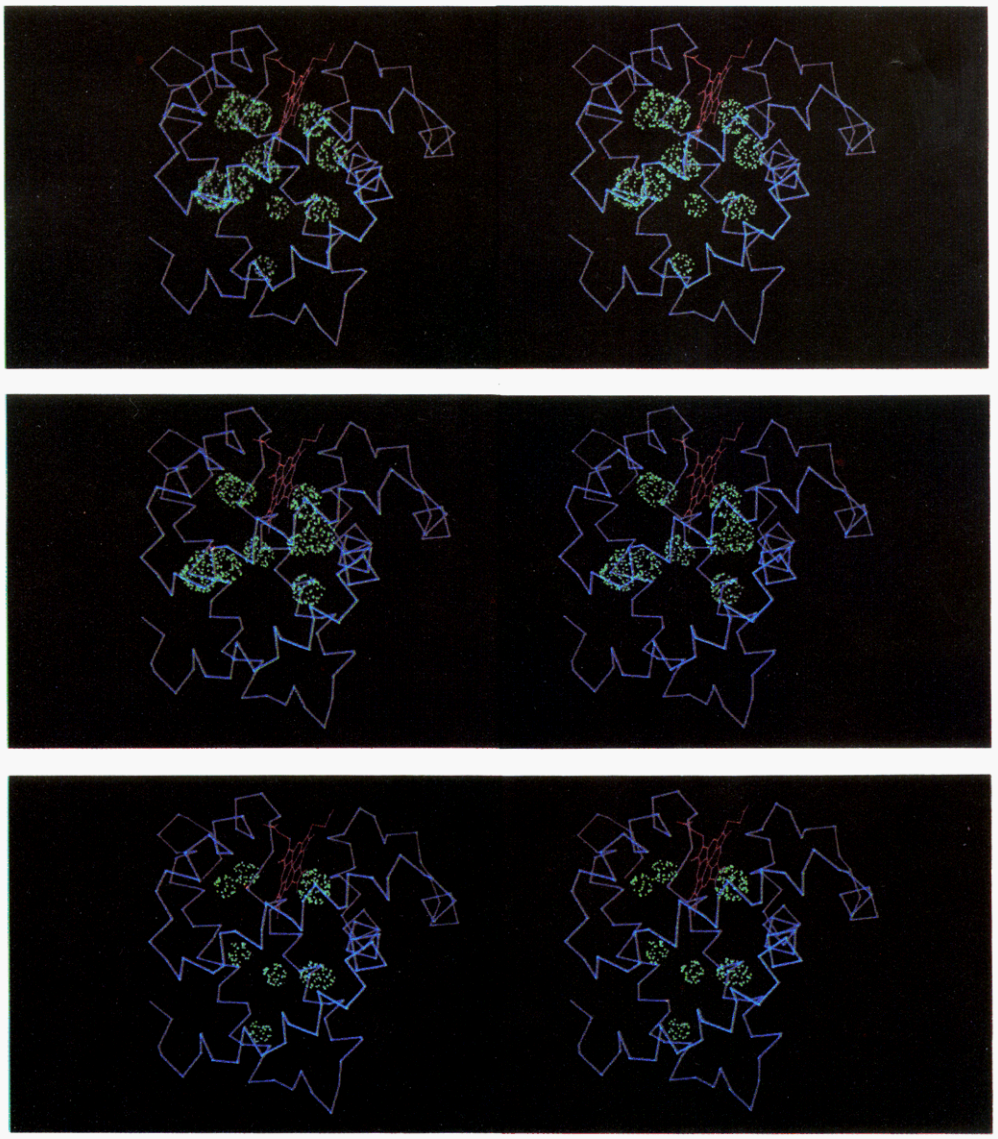

FIGURE 4: Calculated internal cavities of (upper) Mb (270 K), (middle) Mb – Xe (270 K), and (lower) Mb + Xe (270 K). The water molecule has been removed to visualize the distal cavity. The radius of the probe sphere is 1.2 Å. The Connolly algorithms were used to generate the surface and separate the cavities (Connolly, 1983).

atoms but is somewhat larger. To illustrate the distribution of temperature factors, a histogram of the number of protein atoms vs. *B* factor is shown in Figure 8 for metmyoglobin (270 K) and metmyoglobin–Xe (270 K). While the half-width of the distribution is the same for the two structures, we do observe a small redistribution to lower temperature factors in the metmyoglobin–Xe structure.

Discussion

We will divide the discussion into two parts. The first section analyzes the structural features of the metmyoglobin–Xe complex, and the second section compares the xenon

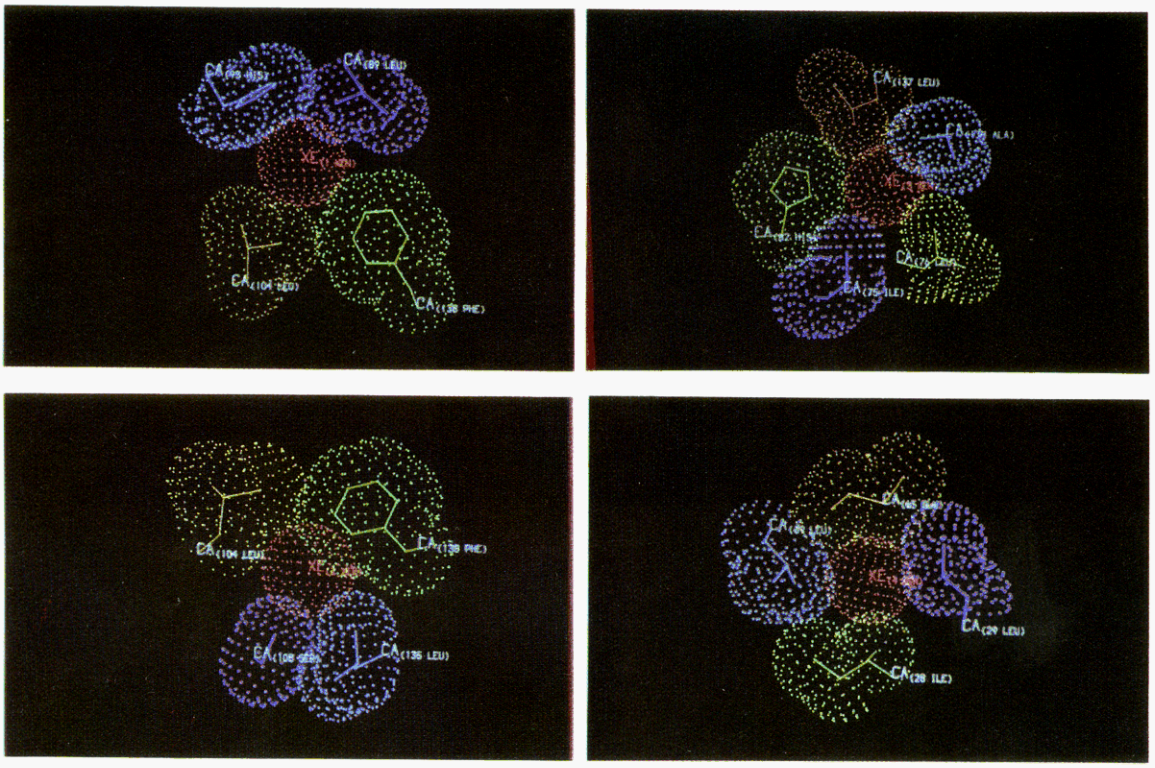

FIGURE 5: van der Waals surface of the xenon atom and surrounding protein atoms for (upper left) site 1, (upper right) site 2, (lower left) site 3, and (lower right) site 4. The xenon atom is colored red. The algorithm to produce these surfaces was written at the UCSF Computer Graphics Laboratory (Bash et al., 1983).

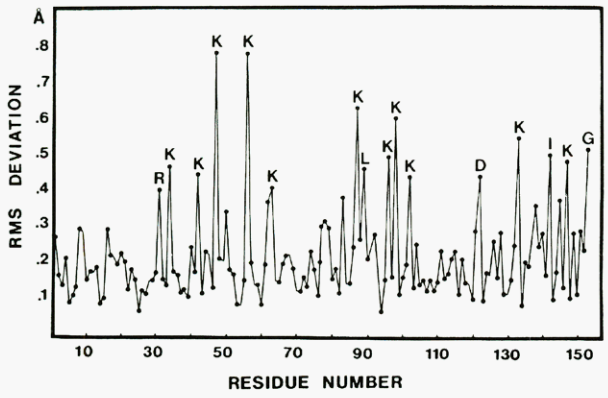

FIGURE 6: Root mean square deviation between metmyoglobin–xenon (270 K) and metmyoglobin (270 K). The rms deviation is averaged over all atoms in each amino acid residue. Residues with an average rms deviation greater than 0.4 Å are identified with the one-letter amino acid code: arginine = R, lysine = K, glutamic acid = E, aspartic acid = D, glycine = G, leucine = L, and isoleucine = I.

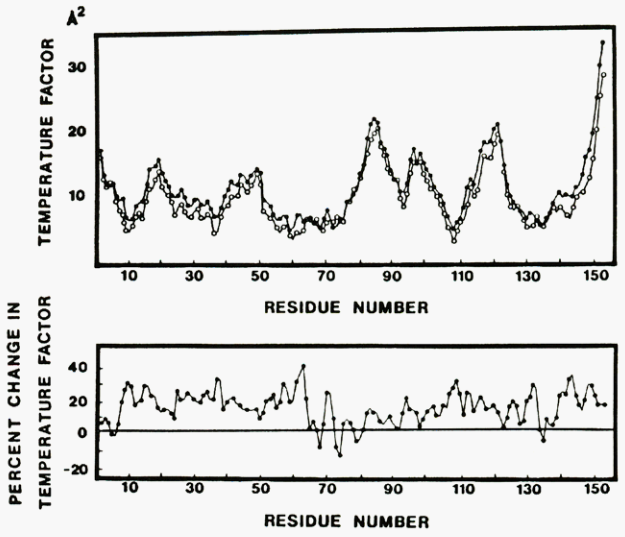

FIGURE 7: (Upper) Refined protein temperature factors averaged over the backbone atoms (C, N, C_α) for each amino acid residue in the metmyoglobin (270 K) (●) and metmyoglobin–xenon (270 K) (○) structures. The temperature factor is related to positional uncertainty by the equation $B = 8\pi^2\langle x^2\rangle$, where $\langle x^2\rangle$ is the mean square displacement for the particular atom. (Lower) Percentage reduction in average backbone temperature factors, [Mb (270 K) − Mb + Xe (270 K)]/Mb (270 K), as a function of residue number.

binding sites observed in the crystal structure with those suggested by solution NMR studies.

An analysis of the metmyoglobin–Xe (270 K) complex and the metmyoglobin (270 K) structure suggests two conclusions. The first is that atom size voids exist within the globin structure that can be filled by small ligands with minimal perturbation of the protein structure. The second is that the specific binding of such ligands tends to decrease the atomic motions reflected in refined atomic temperature factors.

The small rms deviation between metmyoglobin (270 K) and metmyoglobin–Xe (270 K) indicates that only minor structural rearrangements around the Xe binding sites are needed to provide the necessary volume for the binding of a xenon atom (R = 2.10 Å, volume ~39 Å^3). This evidence, combined with the observation that the xenon atoms occupy the internal cavities in metmyoglobin, strongly supports the idea that internal cavities exist in the absence of ligand and are distributed throughout the protein matrix. This is a surprising result in light of the old adage that "nature abhors a vacuum"; however, in the case of the globins we ascribe the internal cavities to a direct consequence of the protein architecture. If such packing defects are then a necessary result of the protein fold and the particular amino acid sequence, we must address the question of the energetics of leaving the cavity unfilled or allowing solvent molecules to fill the space. Two lines of evidence suggest that water molecules do not fill

Table III: Distances between Xe and Protein Atoms and between Equivalent Protein Atoms in Metmyoglobin–Xe (270 K) and Metmyoglobin (270 K) Structures[a]

sequence no.	residue name	atom name	distance between Xe and protein atom in Mb–Xe (270 K)	distance between Xe and protein atom in Mb (270 K)[b]	distance between equiv protein atoms in Mb–Xe (270 K) and Mb (270 K)
xenon 1					
89	Leu (F4)	CG	4.35	3.65	0.71
89	Leu (F4)	CD1	4.65	4.14	0.53
89	Leu (F4)	CD2	3.41	2.33	1.16
104	Leu (G5)	CD1	3.94	4.09	0.61
138	Phe (H14)	CD1	5.60	5.63	0.43
138	Phe (H14)	CD2	5.85	5.58	0.47
138	Phe (H14)	CE1	4.39	4.34	0.62
138	Phe (H14)	CE2	4.66	4.28	0.59
138	Phe (H14)	CZ	3.82	3.51	0.71
142	Ile (H18)	CG1	4.68	4.84	0.78
142	Ile (H18)	CD1	4.05	4.22	1.29
xenon 2					
104	Leu (G5)	CD1	4.22	4.79	0.61
138	Phe (H14)	CD1	2.47	2.19	0.43
138	Phe (H14)	CD2	4.86	4.48	0.47
138	Phe (H14)	CE1	2.78	2.46	0.62
138	Phe (H14)	CE2	5.03	4.66	0.59
138	Phe (H14)	CZ	4.16	3.79	0.71
142	Ile (H18)	CD1	5.01	6.08	1.29
xenon 3					
137	Leu (H13)	CB	4.35	4.69	0.45
137	Leu (H13)	CG	4.24	4.82	0.63
137	Leu (H13)	CD1	5.73	6.28	0.57
137	Leu (H13)	CD2	4.11	4.48	0.53
138	Phe (H14)	CD1	5.81	6.06	0.43
138	Phe (H14)	CD2	4.83	5.11	0.47
xenon 4					
28	Ile (B9)	CG2	3.39	3.71	0.43
68	Val (E11)	CG1	3.43	3.93	0.55

[a] Only atoms that have moved by more than 0.4 Å and are within 6.0 Å of the xenon atom in the metmyoglobin–Xe structure are included. [b] Xenon atom position is assumed from metmyoglobin–Xe (270 K) structure.

these voids in the myoglobin molecule. First, the cavities have a large nonpolar surface area being bordered by leucine, isoleucine, valine, and phenylalanine, and hence a localized water molecule would sacrifice favorable H bonding to gain weaker London dispersion forces. Diffraction studies, which have localized over 40 external waters, do not detect internally bound waters in the myoglobin molecule, implying that the water occupancy is less than 0.1 or that the thermal factors are very high (Hanson & Schoenborn, 1981). While it appears that water molecules do not bind strongly to the interior of the myoglobin molecule, there is strong evidence that water and other ligands are able to penetrate virtually all regions of the protein matrix (Benson et al., 1973). This phenomenon must involve protein fluctuations and transient ligand occupancy in thermodynamically unfavorable locations and hence may not be directly related to the static picture observed in diffraction experiments.

The four bound xenon atoms are observed to occupy a large fraction of the interior volume calculated by the Connolly–Max algorithm (Table II). While all of the larger cavities are observed to bind xenon, the sites do not have equal occupancy even at a xenon gas pressure of 7 atm. There must be a significant contribution to the 2–3 kcal/mol binding energy (Ewing & Maestas, 1970) from both general dispersion interactions and an explicit polarization term. It is curious that while we observe xenon atoms in the four major "nonphysiological" cavities, xenon was not found to bind in the unoccupied distal cavity of deoxymyoglobin (Schoenborn & Nobbs, 1966). Since the cavity appears to be sterically allowed, one explanation is that a lower Xe gas pressure was used in the deoxymyoglobin study, and hence the site was only weakly populated.

One xenon site that is explicitly not observed in this metmyoglobin–Xe crystal structure is in a region formed by the A–B and G–H helix corners. This site was obseved to have nearly 50% occupancy in alkaline myoglobin (Schoenborn, 1969). While it is possible that the occupancy of this site could be dramatically altered at pH 9.1, without protein structural changes, this does not seem to be the case. Instead, the evidence suggests that the alkaline conditions deprotonate histidine-119 (GH1), resulting in the disruption of stabilizing electrostatic interactions. This disruption leads to protein structural changes in the A–B and G–H corners as well as in the E helix and the creation of a new cavity capable of binding a Xe atom. The deprotonation of histidine-119 (GH1) moves the C_α approximately 1 Å and causes a rotation about the C_α–C_β bond of 65°, thus creating a conformational switch, which only opens a transient xenon binding site when the histidine is deprotonated. This idea of protein motions and conformational changes being linked to transient structural defects or cavities is not a new idea but is intriguing as a prototype of gated ligand movement in proteins (Lumry & Rosenberg, 1975).

The refined thermal factors for the xenon atoms range from 19 Å^2 for xenon 1 to 50 Å^2 for xenon 2. Xenon 1, implicated as the tightest binding of the xenon atoms, has a B factor that is 60% higher than the surrounding covalently bonded protein atoms but is still lower than many of the atoms on the surface of the molecule. Xenon 2 has the largest thermal factor and, in the refined geometry, two short protein contacts. These

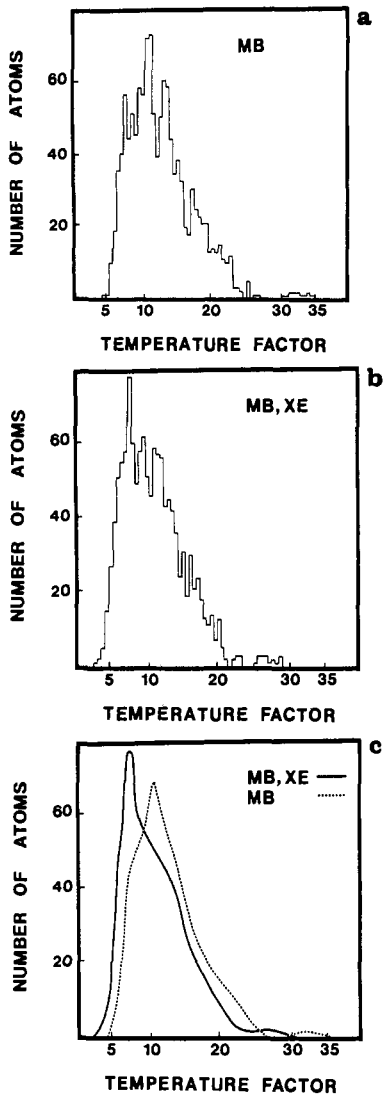

FIGURE 8: Histograms of the number of protein atoms within a given temperature factor range: (a) metmyoglobin (270 K); (b) metmyoglobin–xenon (270 K); (c) smoothed distribution curves for metmyoglobin (270 K) and metmyoglobin–xenon (270 K).

could result in a confined environment producing a disordered xenon 2 binding site or a highly mobile xenon atom. Xenon 3 and xenon 4 have moderate temperature factors of 30 Å^2 that are not unreasonable considering the noncovalent, weak binding nature of sites 3 and 4.

Thermal factors have been of recent interest as measures of dynamic and conformational disorder (Frauenfelder et al., 1979). What are the effects of the binding of noncovalent, uncharged ligands on the thermal factors of a protein? Our observations suggest that there is a small reduction in temperature factor upon ligation that tends to involve large regions of the protein. Superimposed on this small reduction are larger individual residue reductions. For example, the temperature factor decreases for residues histidine-93 (F8), isoleucine-142 (H18), and phenylalanine-138 (H14) can be explained as a local effect if we assume that filling a cavity reduces the motion of surrounding atoms. However, this simple neighbor effect is not sufficient to explain the overall regional reductions. This more general phenomenon could arise if there were a ligand-induced restriction of the number of conformational substates, i.e., a "freezing-in" of ligand-stabilized substates. Conformational substates have been postulated for CO-deoxymyoglobin (Austin et al., 1975) and Xe–CO-deoxymyoglobin (Yue, 1983) on the basis of kinetic evidence. We stress that a 13% reduction in average *B* factor is not a large effect, and we consider the present evidence to be suggestive but not definitive.

The fact that we do not observe full occupancy in the four xenon sites leads to a number of questions. The first pertains to which sites are actually occupied for any one metmyoglobin molecule. Clearly all four sites are available, but just as clearly, 7 atm of xenon gas pressure is not sufficient to occupy simultaneously all sites in all of the myoglobin molecules. On average, at least two sites are occupied at any one time in all of the myoglobin molecules, and with the assumption of independent xenon sites, 12% of the myoglobin molecules would have all four sites filled at this Xe gas pressure. There exists some solution binding evidence for cooperativity between xenon sites in CO-myoglobin (Settle, 1971).

A second ambiguity arises in the structural analysis of the xenon 2 site, particularly in the close contacts observed between the xenon atom and phenylalanine-138 (H14). We believe we are observing the average position of the side-chain conformations with xenon present and absent. Xenon could be most simply accommodated by a further rotation about the C_α–C_β bond, i.e., greater than the 12° observed between metmyoglobin–Xe (270 K) and metmyoglobin (270 K). This would remove the unfavorable steric contacts with the Xe atom. The conformation with the Xe absent could be the same as that observed in metmyoglobin (270 K), which would result in very short Xe–Phe-138 (H14) contacts (Table III). This postulate is difficult to confirm at 1.9-Å resolution, since we are unable to distinguish the two alternate conformations in the electron density maps.

A final caveat regarding the partially occupied xenon sites is that the refined protein atomic temperature factors result from a statistical average over a large number of motional and conformational states of myoglobin in the absence or presence of the various bound xenon atoms. This will have two effects. First, the observed refined *B* factors will be an overestimation of the protein *B* factors of the bound state, if indeed Xe binding decreases protein conformational states. Second, it makes a detailed mechanistic understanding of the regional and global changes quite difficult. These problems are unfortunately inherent in any partial occupancy experiment. One obvious solution would be to increase the occupancy of sites 2, 3, and 4 by increasing the pressure of xenon gas.

Comparison with NMR Results. Although the experimental conditions are very different, we can use these crystallographic results to help interpret recent NMR studies of the metmyoglobin–Xe complex (Tilton & Kuntz, 1982). The NMR studies distinguish two families of sites for xenon binding to metmyoglobin. Xenon in the first class of sites has a measured kinetic off rate of 1×10^{-5} M/s, is sensitive to the paramagnetic Fe atom, and can be effectively displaced with HgI_3^-. The second class has faster binding kinetics, is distant from the Fe, and is only weakly affected by HgI_3^- binding. A comparison of these environmental and kinetic parameters with the metmyoglobin–Xe crystal structure allows us to make more definitive statements. While class 1 was originally believed to occupy only the proximal cavity, we now think that the NMR studies measure an average of X-ray sites 1 and 2. Not only are both sites relatively close to the Fe and to each other but also they occupy nearly the same positions as two of the iodine atoms of bound HgI_3^- (Kretsinger et al., 1968). Thus it now appears that HgI_3^- may compete effectively with Xe for binding sites 1 and 2. The second xenon binding class detected in the NMR studies was believed to be in the A–B, G–H corner region. There were three reasons for this assignment. First, a site close to the surface explained

the observation of faster kinetics. Second, the ^{129}Xe NMR signal is shifted downfield from ^{129}Xe in water, as is the ^{129}Xe signal in hemoglobin. Third, this site was the only other identified Xe binding site in the globins. While we cannot unambiguously rule out the possiblity of this site existing in solution, the crystal structure strongly suggests an alternative interpretation. Xenon 3 resides in a cavity near the surface that is separated from solvent by alanine-134 (H10) and glycine-80 (EF3) and hence appears to be relatively accessible. This site is 13.5 Å from the Fe and would only weakly sense the paramagnetic effects. While this xenon site satisfied the NMR criteria, we reiterate that we have no direct proof that it is responsible for the NMR signals. Finally, xenon 4 is still somewhat of a mystery. It is relatively close to the Fe and appears to be deeply buried on the distal side of the molecule away from the HgI_3^- binding site. We have no NMR evidence for the existence of this site. Unfortunately, there are no reported alternative ligands for xenon sites 3 and 4 that can be used cleanly in a direct competition experiment. Perhaps solid-state NMR techniques could be of value in unraveling these questions.

Direct comparison of the solution NMR and crystallographic results must be approached with caution. While it is generally recognized that the solution and crystal structures are very similar, it has not been demonstrated that the population distribution of conformational substates is the same. The high salt environment (4.0 M ammonium sulfate) of the crystal study may alter the electrostatic interactions that mediate ligand binding. Effects of this kind are seen with alkaline myoglobin, which involve the equilibrium position of histidine-119 (GH1). If this equilibrium were also sensitive to ionic strength, we would alter the preferred Xe binding sites. We have examined the solution ^{129}Xe NMR of metmyoglobin in 50% saturated ammonium sulfate. Our data are similar to the dilute salt studies and show HgI_3^- competition for xenon. However, some quantitative differences exist and no definitive interpretation can be made about the effects of high salt on Xe binding sites or binding affinities (R. F. Tilton and I. D. Kuntz, unpublished results).

Finally, in comparing the two experiments, we must recognize the limitations of the techniques. While X-ray crystallography is able to locate precisely the individual atoms, there must be a significant localized population to be observed. For the xenon atom the occupancy would have to be at least 10% with even a moderate temperature factor of 20 Å^2. Thus, if a xenon site is only weakly populated or highly mobile, it is likely to be missed in an X-ray crystallographic experiment. On the other hand, NMR can be very sensitive to low occupancy if the chemical shift difference for the sampled environments is large. Since xenon has a substantial chemical shift range of $\sim$100 ppm in metmyoglobin (20 ppm downfield to 80 ppm upfield from xenon in H_2O), the observed average resonance frequency $\Delta\nu$ could show population changes of $<5\%$. However, while NMR is capable of detecting weakly populated sites, it cannot differentiate environments with similiar chemical shifts. Moreover, the fast exchange on the NMR time scale of the Xe atom among the various protein sites forms a single averaged resonance from which it is difficult to extract specific binding site information. Even with these limitations and potential difficulties the NMR and crystallographic tools can be combined to provide a clearer understanding of small molecule–protein interactions.

There are two important questions that we do not directly address in this study. The first concerns the implication of small packing defects and the effects of filling these defects on the functional O_2 binding properties of myoglobin. The second concerns the protein dynamics and transient pathways that control the movement of small ligands in the protein matrix. While equilibrium binding studies have shown that Xe binding reduces the CO binding affinity by 75% (Settle, 1971), crystallographic studies have indicated that Xe is not in direct competition for the O_2 cavity (Schoenborn & Nobbs, 1966). We can suggest a few possibilities for the observed allostery. One possibility is that xenon 1, which fills the proximal cavity, makes numerous van der Waals contacts with the proximal histidine-93 (F8). These direct interactions may provide enough steric hindrance to prevent proper movement and reorientation of the histidine as it is pulled/pushed toward the plane of the heme ring upon CO ligation and the resulting transition from Fe^{2+} ($S = 2$) to Fe^{2+} ($S = 0$). A second possibility is that xenon 4, which binds in a cavity directly below the O_2 binding site, is able to disrupt the structural rearrangements during the gating motions of residues controlling ligand entry. A third possibility is that there are no direct interactions between the Xe atom and CO or between a Xe atom and a successive linkage of protein atoms to the distal cavity, but instead the binding of ligands in cavities restrains the protein by altering the intricate and subtle energetics involved in the ligand–protein binding interactions. The observation that interior spaces are redistributed upon the addition of Xe and the regional reductions in temperature factors supports this type of idea.

We are unable to say anything definitive about the role of the protein on ligand mobility. A variety of cooperative protein fluctuations are surely implicated, but it is not clear if an accurate picture of these protein dynamics can be gleaned from the static structure observed in X-ray crystallographic studies. A preliminary study seems to indicate that a large number of small internal channels are present in the static structure, which connect the internal cavities with each other and with the surface of the protein (I. D. Kuntz, N. Max, and R. F. Tilton, unpublished results). These channels and the presence of internal cavities support a plausible mechanism of "mobile defects", a field that is still poorly understood but is worthy of further investigation.

Conclusion

Four xenon binding sites with occupancy between 0.45 and 1.0 are located inside the metmyoglobin molecule by X-ray crystallography. The sites are located in small packing defects and are distributed throughout the protein matrix. The metmyoglobin–xenon structure is essentially isomorphous with respect to the reference metmyoglobin structure but has lower refined protein temperature factors by 10–15%. The small effects of xenon binding on the protein structure support the idea that the internal cavities are present in native metmyoglobin. The regional decrease of the temperature factors argues for a ligand-induced restriction of conformational substates.

Acknowledgments

We thank Robert Stroud, Peter Kollman, Benno Schoenborn, Mel Jones, Mike Connolly, Paul Bash, Peter Desmeules, Steve Sprang, and Willa Crowell for their contributions during the project. A special thanks is due to the members of G.A.P.'s laboratory for their hospitality during the data collection visits of R.F.T.

Supplementary Material Available

Tables containing interaction distances between xenon 1–4 and protein atoms (3 pages). Ordering information is given

on any current masthead page.

References

Austin, R. H., Beeson, K. W., Eisenstein, L., Frauenfelder, H., & Grunsalus, I. C. (1975) *Biochemistry 14*, 5355–5373.

Bash, P., Pattabiraman, N., Huang, C., Ferrin, T., & Langridge, R. (1983) *Science (Washington, D.C.) 222*, 1325–1327.

Benson, E. S., Rossi Fanelli, M. R., Giacometti, G. M., Rosenaberg, A., & Antonini, E. (1973) *Biochemistry 12*, 2699–2706.

Connolly, M. (1981) Ph.D. Thesis, University of California, San Francisco.

Connolly, M. (1983) *Science (Washington, D.C.) 221*, 709–713.

Ewing, G. J., & Maestas, S. (1970) *J. Phys. Chem. 74*, 2341–2344.

Frauenfelder, H., Petsko, G. A., & Tsernglou, D. (1979) *Nature (London) 280*, 563–588.

Hanson, J. C., & Schoenborn, B. P. (1981) *J. Mol. Biol. 153*, 117–146.

Kendrew, J. C., & Parrish, R. G. (1956) *Proc. R. Soc. London, Ser. A 238*, 305–324.

Konnert, J. H., & Hendrickson, W. A. (1980) *Acta Crystallogr., Sect. A A36*, 344–350.

Kretsinger, R. H., Watson, H. C., & Kendrew, J. C. (1968) *J. Mol. Biol. 31*, 305–314.

Lumry, R., & Rosenberg, A. (1975) *Colloq. Int. CNRS 246*, 53–62.

North, A. C., Phillips, D. C., & Mathews, F. S. (1968) *Acta Crystallogr., Sect. A A24*, 351–359.

Richards, F. M. (1977) *Annu. Rev. Biophys. Bioeng. 6*, 151–176.

Schoenborn, B. P. (1965) *Nature (London) 208*, 760–762.

Schoenborn, B. P. (1969) *J. Mol. Biol. 45*, 297–303.

Schoenborn, B. P., & Nobbs, C. L. (1966) *Mol. Pharmacol. 2*, 495–498.

Schoenborn, B. P., Watson, H. C., & Kendrew, J. C. (1965) *Nature (London) 207*, 28–30.

Settle, W. (1971) Ph.D. Thesis, University of California, San Francisco.

Takano, T. (1977) *J. Mol. Biol. 110*, 537–568.

Tilton, R. F., & Kuntz, I. D. (1982) *Biochemistry 21*, 6850–6857.

Yue, K. T. (1983) Ph.D. Thesis, University of Illinois, Urbana.

Absence of Cooperative Energy at the Heme in Liganded Hemoglobins†

D. L. Rousseau,* S. L. Tan,‡ M. R. Ondrias,§ S. Ogawa, and R. W. Noble

ABSTRACT: Using resonance Raman and infrared absorption spectroscopies, we show that there are no energetically significant structural changes at the heme upon the quaternary structure transition in six-coordinate hemoglobins. These observations are at variance with the presently accepted mechanism for cooperativity, which postulates severe strain in the T quaternary structure of liganded hemoglobin. By consideration of the present results, and studies on deoxyhemoglobins and photodissociated hemoglobins, a view of the distribution of the free energy of cooperativity emerges. In five-coordinate deoxyhemoglobins the iron–histidine bond is able to respond to the protein structure, thereby accounting for a wide variation (40 cm^{-1}) in its frequency. In contrast, when a sixth ligand is present and the iron is pulled into plane, the histidine–heme–ligand complex becomes structurally rigid, thereby preventing protein-induced changes at the heme. Instead, in liganded hemoglobin the changes in structure that occur at the subunit interface upon the quaternary structure transition are accommodated away from the heme by relatively weak bonds in the protein.

Despite many years of study, the molecular basis for cooperativity in hemoglobin is not understood (Rousseau & Ondrias, 1983). This results in part from the difficulty of studying all of the many possible interactions that could contribute to cooperativity. As a starting point, the quaternary structure dependent interactions at the binding site, i.e., the heme–protein–ligand interactions, must be elucidated. Only then can the amount of cooperative energy localized at the heme be evaluated and routes of information transfer within the tetramer be revealed. In order to study protein–heme interactions it is helpful to consider independently three separate regions of the heme pocket that may contribute to ligand stabilization and cooperative pathways: the proximal histidine–heme interaction; the interaction between the protein environment and the bound ligand; and direct interactions between the protein and the porphyrin. Additionally, in an assessment of the energetics of cooperativity, it is necessary to examine both liganded and deoxyhemoglobins (Ondrias et al., 1982). The effect at the heme of the quaternary structure transition in both deoxyhemoglobins (Ondrias et al., 1983; Nagai & Kitagawa, 1980; Nagai et al., 1980b) and methemoglobins (Henry, 1980; Nagai et al., 1980a; Scholler & Hoffman, 1979; Asher, 1981) has been extensively examined with resonance Raman scattering. Relatively few analogous studies of ferrous liganded hemoglobins have been reported (Nagai et al., 1980b; Tsubaki et al., 1982).

The importance of studying ferrous liganded hemoglobins becomes clear when the various mechanisms of cooperativity are considered. It is generally viewed that in the deoxy protein there is very little quaternary structure dependent strain at the heme but in liganded hemoglobin there is considerable strain (Baldwin & Chothia, 1979; Dickerson & Geis, 1983).

† From AT&T Bell Laboratories, Murray Hill, New Jersey 07974 (D.L.R., S.L.T., M.R.O., and S.O.), and the Department of Medicine and Biochemistry, State University of New York at Buffalo, and the Veterans Administration Medical Center, Buffalo, New York 14215 (R.W.N.). *Received November 4, 1983.* R.W.N. is a recipient of USPHS Grant HL-12524 and is supported also by a research fund from the Veterans Administration.

‡ Present address: Department of Chemistry, Massachusetts Institute of Technology, Cambridge, MA 02139.

§ Present address: Department of Chemistry, University of New Mexico, Albuquerque, NM 87131.

0006-2960/84/0423-2857$01.50/0